PHYSICAL REVIEW A VOLUME 48, NUMBER 4 OCTOBER 1993

Semiclassical description of antiproton capture on atomic helium

W. A. Beck
Department of Physics, University of Washington, Seattle, Washington 98195
and Quantum Medical Systems, Issaquah, Washington 98027

L. Wilets
Department of Physics, University of Washington, Seattle, Washington 98195

M. A. Alberg
Department of Physics, University of Washington, Seattle, Washington 98195
and Department of Physics, Seattle University, Seattle, Washington 98122
(Received 19 April 1993)

A semiclassical, many-body atomic model incorporating a momentum-dependent Heisenberg core to stabilize atomic electrons is used to study antiproton capture on helium. Details of the antiproton collisions leading to eventual capture are presented, including the energy and angular-momentum states of incident antiprotons which result in capture via single- or double-electron ionization, i.e., into $He^{2+}\,\bar{p}$ or $He^{+}\,\bar{p}$, and the distribution of energy and angular-momentum states following the Auger cascade. These final states are discussed in light of recently reported, anomalously long-lived antiproton states observed in liquid He [Iwasaki *et al.*, Phys Rev. Lett. **67**, 1246 (1991)].

PACS number(s): 36.10.−k, 25.43.+t, 34.10.+x

I. INTRODUCTION

The "trapping" of antiprotons stopped in liquid He into long-lived states has been reported recently by Iwasaki *et al.* [1]. Approximately 3.6% of the incident antiprotons exhibit delayed decay, of the order of microseconds compared with picoseconds for prompt decays, opening possibilities for further experimentation, including antihydrogen production.

The initial slowing and capture of in-flight antiprotons is via energy loss due to Auger excitation and ionization of the atomic electrons, while the later stages are dominated by radiation, and eventual annihilation. Auger transitions are characteristically many orders of magnitude more rapid than radiative decay, making the dynamics of the Auger process central to understanding the delayed antiproton annihilation.

Yamazaki *et al.* [2], following the work of Condo [3] and Russell [4], proposed that the long-lived antiprotons were captured into "metastable, circular states," of principal quantum number $n_0 = \sqrt{M^*/m_e} \approx 38$ and with $\ell_0 \approx n_0 - 1$, of the exotic neutral $He^{+}\,\bar{p}$ atom. ($M^* = 4M_{\bar{p}}/5$ is the antiproton reduced mass with respect to He and m_e is the electron mass.)

From these states further Auger transitions would be highly inhibited: (1) $\Delta\ell > 1$ is highly unfavored and the atomic excitation energies are large compared with the antiproton spacing for $\Delta n = \Delta\ell = -1$, and (2) the Stark effect, which normally admixes $\ell = 0$ states due to the presence of other atoms in the liquid and enhances $\bar{p}$ annihilation in the nucleus for atoms stripped of inner electrons, is suppressed due to the removal of ℓ degeneracy by the presence of the remaining electron.

Thus decay is limited to the much slower radiative transitions, which have small photon energy, and antiproton annihilation is delayed.

In order to study the capture of antiprotons by He atoms, we have modeled antiproton collisions with He using a classical description of the antiprotons and a semiclassical description of the electrons, in which the electrons of the target system are stabilized by a momentum-dependent Heisenberg core [5]; the Pauli principle can be ignored here since the atomic electrons are in antiparallel states.

There is a long history of studies of the formation of exotic atoms, dating back to the pioneering work of Fermi and Teller [6], who considered the electron cloud to be a viscous fluid which slowed and led to eventual capture of the exotic projectiles. The process of slowing down and capture is generally understood, but detailed agreement with experiment remains elusive. Important contributions have been made by many researchers, including Haff and Tombrello [7] and Leon [8]. An excellent compendium is to be found in [9].

Various classical-trajectory Monte Carlo calculations [10–13], and especially those of Cohen [14], have looked at the capture of exotic particles on small atoms, using a mean electric field to approximate the atomic structure, while semiclassical treatments of larger systems have used various quantum mechanical approximations of atomic structure with which the classical exotic particle interacts [15–23]. The approach used in this work employs a consistent semiclassical treatment: whereas a classical atom prepared in a state with a momentum distribution (to simulate the quantum distribution) evaporates outer electrons while inner electrons collapse into the nucleus, the Heisenberg core used here prevents this. This approach has had considerable success, when com-

bined with a similar momentum-dependent Pauli core to hold like electrons apart in phase space, in describing atomic ground states [5], electron-transfer reactions [24], stopping power [25], etc.

II. QUANTUM AND ADIABATIC SOLUTIONS OF THE He-$\bar{p}$ SYSTEM

Consider now the quantum states of this system, an exotic "molecule" consisting of the He nucleus, i.e., an α particle, the antiproton and N =0, 1, or 2 electrons. Working in atomic units, with $\hbar = m_e = e = 1$ (ignoring the negligible effect of electron reduced mass), the Hamiltonian is given by

$$H = \frac{P^2}{2M^*} - \frac{2}{R} + \sum_{i=1}^{N}\left[\frac{p_i^2}{2} - \frac{2}{r_i} + \frac{1}{|\mathbf{R}-\mathbf{r}_i|}\right] + \frac{1}{r_{12}}\delta_{N,2}\,, \tag{1}$$

where $\mathbf{r}_i$ and $\mathbf{R}$ are the electron and antiproton coordinates relative to the helium nucleus, and $\mathbf{p}_i$ and $\mathbf{P}$ are the corresponding momenta; $M^* = 1469$ is the reduced mass of the antiproton in atomic units.

The zero electron (double ionization) problem is simply the He^+ ion with the $\bar{p}$ replacing the electron. The energy levels are given by

$$E_n = -\frac{Z^2 M^*}{2n^2} = -\frac{2M^*}{n^2}\,. \tag{2}$$

Note that $n_0 = \sqrt{M^*} \approx 38$ corresponds to a $\bar{p}$ orbit of the same size and energy as the $1s$ electron orbit; because of the large M^* and consequent large quantum numbers for the antiproton states of interest, the antiproton may be treated classically.

The one electron (single ionization) problem is described well in the adiabatic Born-Oppenheimer approximation. We note that this two-center, one-electron problem is separable in prolate spheroidal coordinates and can thus be calculated to high accuracy; cf. [26, 27]. In terms of the coordinates defined above, the energy levels $\varepsilon_n(R)$ of one electron in the potential of the He nucleus and fixed antiproton are given by

$$\left[\frac{p^2}{2} - \frac{2}{R} - \frac{2}{r} + \frac{1}{|\mathbf{R}-\mathbf{r}|}\right]\psi_n(\mathbf{r},\mathbf{R}) = \varepsilon_n(R)\psi_n(\mathbf{r},\mathbf{R}) \tag{3}$$

and are the potential energy for the Born-Oppenheimer antiproton eigenvalue equation,

$$\left[\frac{P^2}{2M^*} + \varepsilon_n(R)\right]\Phi_{n,m}(\mathbf{R}) = E_{n,m}\Phi_{n,m}(\mathbf{R})\,. \tag{4}$$

Here $P^2 = -R^{-1}(\partial^2/\partial R^2)R + L^2/R^2$ includes vibrational and rotational excitation. These Born-Oppenheimer states are not stationary states of the full problem, however, since there remain velocity terms in the full Schrödinger equation which couple the adiabatic levels. Quite generally we can expand the total wave function in terms of the eigenfunctions of Eq. (3),

$$\Psi(\mathbf{r},\mathbf{R}) = \sum_n \Phi_n(\mathbf{R})\psi_n(\mathbf{r},\mathbf{R})\,. \tag{5}$$

The Schrödinger equation for the Φ_n is then

$$\left[\frac{P^2}{2M^*} + \varepsilon_n(R) - E\right]\Phi_n + \frac{1}{2M^*}\sum_{n'}\left[2\langle n|\mathbf{P}|n'\rangle\cdot\mathbf{P} + \langle n|P^2|n'\rangle\right]\Phi_{n'} = 0\,, \tag{6}$$

where $|n\rangle$ corresponds to ψ_n and the bra-ket integration is over $\mathbf{r}$.

In a time-dependent calculation, these coupling terms lead to Auger transitions between the adiabatic states. Note that the first coupling term is essentially of the dipole form (the operator is $\mathbf{P}$). Thus transitions with $|\Delta\ell| > 1$ are (progressively more) inhibited.

Alternately, Yamazaki and Ohtsuki [28] have obtained approximate solutions to the Born-Oppenheimer problem using configuration-mixing techniques, in which antiproton states are calculated with the electron in the ground state, and then mixed with excited states of the electron to obtain the system levels shown in Fig. 1. Here, the system levels $L = N - 1$ are proposed as the boundary of the allowed E, L states, with the states with $L > 31$ proposed as the region of metastability.

Because of the infinite range of the central Coulomb potential, the Born-Oppenheimer energy level diagram of $E(L)$, where L is the total angular momentum, in theory extends to the right indefinitely; this can be seen by considering first a simple $\alpha\bar{p}$ state in the energy region covered in Fig. 1. An electron can then be placed in a hydrogenic orbit of arbitrarily small energy and arbitrarily large angular momentum without disturbing the $\bar{p}$. Only some of these states were observed in our calculations.

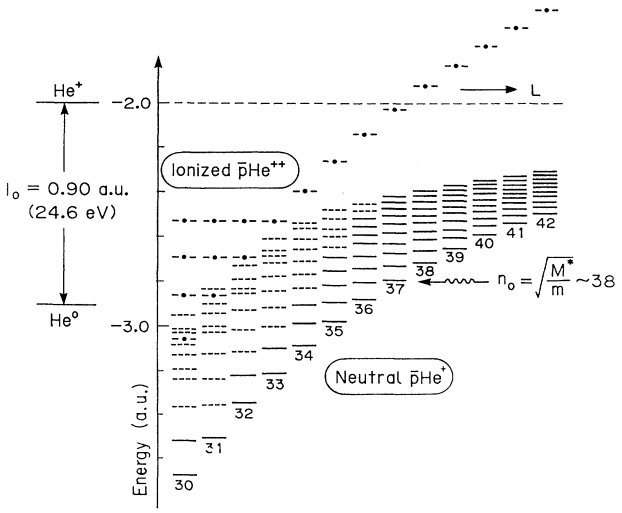

FIG. 1. The energy levels of of the $\alpha e \bar{p}$ system courtesy of Yamazaki and Ohtsuki [28].

Capture of $\bar{p}$ into the two electron negative ion was seldom observed in our calculations; this negatively charged system appeared only briefly during the initial stages of antiproton capture, and was unstable to electron ionization during the antiproton capture and decay process.

III. THE SEMICLASSICAL MODEL

In the semiclassical model [5], the Hamiltonian of the undisturbed helium atom is

$$H_{\rm sc} = \frac{p_1^2}{2} + \frac{p_2^2}{2} - \frac{2}{r_1} - \frac{2}{r_2} + \frac{1}{r_{12}} + V_H \ , \tag{7}$$

with V_H the momentum-dependent Heisenberg core which prevents the collapse of the electrons into the He nucleus, given by

$$V_H = \frac{\xi_H}{4\alpha r^2} \exp\left\{\alpha[1 - (r\,p/\xi_H)^4]\right\} \ . \tag{8}$$

We choose for the model parameters [5] $\alpha = 1.0$, $\xi_H = 2.767$. The Hamiltonian then minimizes at an energy of -2.78 with $r_1 = r_2 = 0.63$, in fair agreement with the exact ground state energy of $-2.9037\ldots$ at an electron mean radius of $\langle r \rangle \approx 0.59$.

The total Hamiltonian is then

$$H_{\rm sc} = \frac{P^2}{2M^*} - \frac{2}{R} + \sum_{i=1}^{2}\left[\frac{p_i^2}{2} - \frac{2}{r_i} + \frac{1}{|\mathbf{R} - \mathbf{r}_i|} + V_H(r_i, p_i)\right] + \frac{1}{r_{12}} \ . \tag{9}$$

To model collisions, Hamilton's classical equations of motion

$$\frac{dx_i}{dt} = \frac{\partial H_{\rm sc}}{\partial p_i} \ , \quad \frac{dp_i}{dt} = -\frac{\partial H_{\rm sc}}{\partial x_i} \tag{10}$$

are solved for $\mathbf{r}_1$, $\mathbf{p}_1$, $\mathbf{r}_2$, $\mathbf{p}_2$, $\mathbf{R}$, $\mathbf{P}$, the coordinates describing our semi-classical system, and integrated over time using the venerable ordinary differential equation routine ODE.

IV. COLLISION CALCULATIONS

Monte Carlo calculations of antiproton collisions with He were performed as follows:

(1) The target He atom was prepared in its ground state with random orientation and parity inversion of the electron coordinates and momenta, as described in [29].

(2) The projectile $\bar{p}$ was launched at this target atom with an initial energy of about 80 eV (about 3.0 a.u.) and with an impact parameter b randomized with equal areas (πdb^2) up to an energy-dependent $b_{\rm max}$.

(3) Sequences of collisions were followed from one encounter to the next until capture occurred.

Our initial energy and $b_{\rm max}$ were chosen so that collisions would never result in antiproton capture on the first encounter, and the final energy of the antiproton after each collision could be used as the starting energy for a subsequent collision, again with Monte Carlo initial conditions for the ground state of the new target and for the new impact parameter.

As the antiproton slowed, $b_{\rm max}$ was increased in stages: we began with $b_{\rm max} = 1.0$; when $\bar{p}$ energies dropped below 2.3 a.u., the level at which small numbers of captures first began to be observed, $b_{\rm max}$ was increased to 2.0; when $\bar{p}$ energies dropped below 1.2, somewhat above the range where capture cross sections began to flatten out with $b_{\rm max}$ of 2.0, $b_{\rm max}$ was increased to 3.0.

While somewhat artificial, by selecting for collisions during which something happened this method allowed us to study a realistic distribution of antiproton projectiles during the last stages of antiproton cascade down to eventual capture, typically after five to twenty sequential collisions, while decreasing the amount of computer time spent modeling weakly interacting collisions of large energy and impact parameter.

A total of 4000 collision sequences (approximately 41 000 individual antiproton-He collisions) were followed. 916, or about 23%, ended with capture via single-electron ionization into the neutral exotic $\alpha e \bar{p}$, while the remaining 77% resulted in capture via double ionization into a positively charged $\alpha\bar{p}$.

Figure 2(a) shows our total energy loss cross sections, $d(\sigma\Delta E)/dE$, of the $\bar{p}$ as a function of initial $\bar{p}$ energy. In the higher energy collisions at the start of a collision sequence, little slowing of the antiprotons occurs for large impact parameters. As the antiprotons slow, energy loss increases at larger impact parameters until the antiprotons drop into the energy range from which capture begins to occur, slightly below the energy at which we first

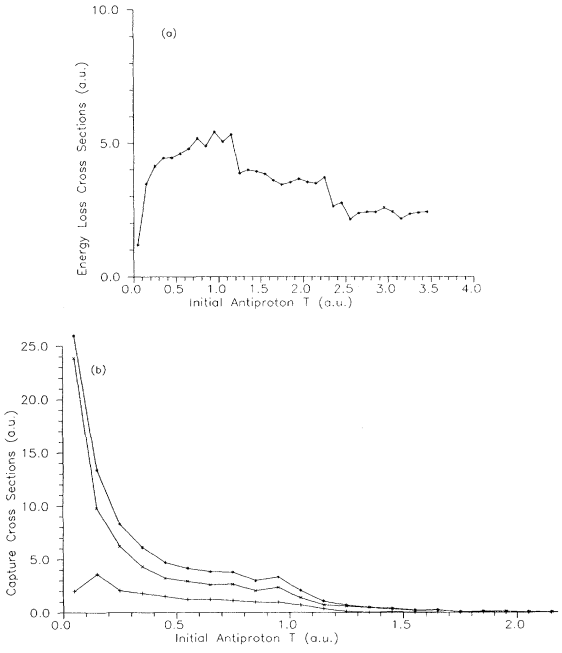

FIG. 2. (a) Energy-loss cross sections for 41 417 $\bar{p}$-He collisions, as a function of initial $\bar{p}$ kinetic energy, T. (b) Capture cross sections for 4000 $\bar{p}$-He collisions, as a function of initial $\bar{p}$ kinetic energy, T. Capture ino $\bar{p}\,e\,\alpha$ states are denoted by (+), into $\bar{p}\,\alpha$ by ($\times$), and total by ($*$).

increased the maximum impact parameter; step increases in these energy loss cross sections are clearly visible at energies of 2.3 a.u. and 1.2 a.u., where we increased the maximum impact parameter.

Figure 2(b) shows our antiproton capture cross sections for these collisions via single and double ionization, again as a function of antiproton energy. As the antiprotons slow, the maximum impact parameter at which capture occurs grows; since the central Coulomb potential of the He nucleus has the form $1/r$, the total capture cross section becomes infinite for very low energies. Here, our total capture cross section levels out to $\pi b_{\max}^2$ at the lowest antiproton energies, where all the antiprotons are captured; our maximum impact parameter of 3.0 for these lower energy collisions was chosen so that this saturation occurred only for $\bar{p}$ energies of approximately 0.1 a.u. or lower.

Due to the limited amount of energy and angular momentum that can be exchanged by the massive antiproton and the bound electrons of the He atom, antiproton energies and angular momenta which result in capture fall into a fairly narrow range, as shown in Figs. 3(a) and 3(b). Figure 3(a) shows the range of incident antiproton energies and angular momenta which result in capture via double-electron ionization; the adjacent range of higher energy and angular-momenta antiprotons which were captured via single ionization is shown in Fig. 3(b).

Figure 4(a) shows the energy and angular momentum of the final states into which the antiproton was captured via double ionization. For capture via single ionization, Fig. 4(b) shows the $\alpha\bar{p}e$ system states; in Fig. 4(c), just the antiproton states of these systems are plotted. Here, after capture the antiproton continues to interact and exchange energy and angular momentum with the remaining electron, so each of states plotted in Fig. 4(c) represents a time average of the antiproton configurations. Figures 5(a), and 5(b), showing the changing electron and antiproton radii as they interact over time, are examples of a typical $\alpha e\bar{p}$ system dynamics after antiproton capture.

Density contours of these scatter plots, in percent of total collisions per unit E per unit L, are combined in Fig. 6, illustrating how the adjacent bands of incident antiprotons of Fig. 3 drop into the captured states of Fig. 4, and the relationship of the states of the antiprotons captured via single ionization to the states of the total system.

Also of interest are the transition E and L distributions of the antiprotons when they are first captured by the He atom. Figure 7(a) shows the initial capture states of the antiprotons in what will become the doubly ionized $\alpha\bar{p}$, when the systemwas an unstable $\alpha e\bar{p}$ or, in some cases, $\alpha ee\bar{p}$. Figure 7(b) shows the higher angular-momentum states of the antiprotons captured into what will become the singly ionized $\alpha e\bar{p}$, again at the point of initial antiproton capture. Comparison with Figs. 3 and 4 shows

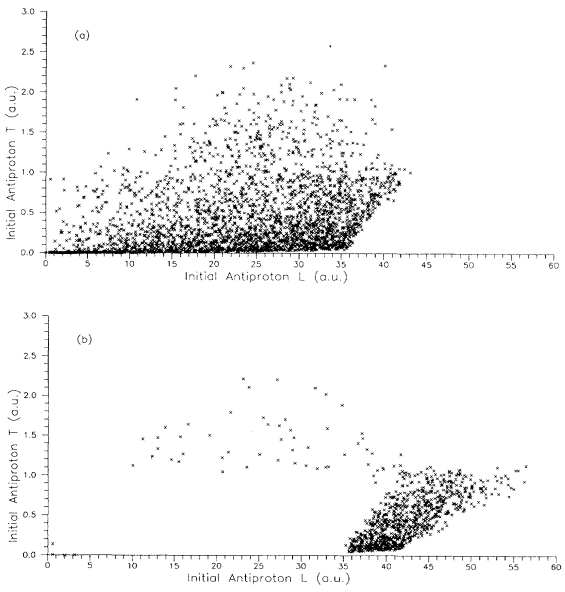

FIG. 3. Initial state of the $\bar{p}$ for the last pass in the cascade before capture into a (a) $\bar{p}\alpha$ state and (b) $\bar{p}e\alpha$ state.

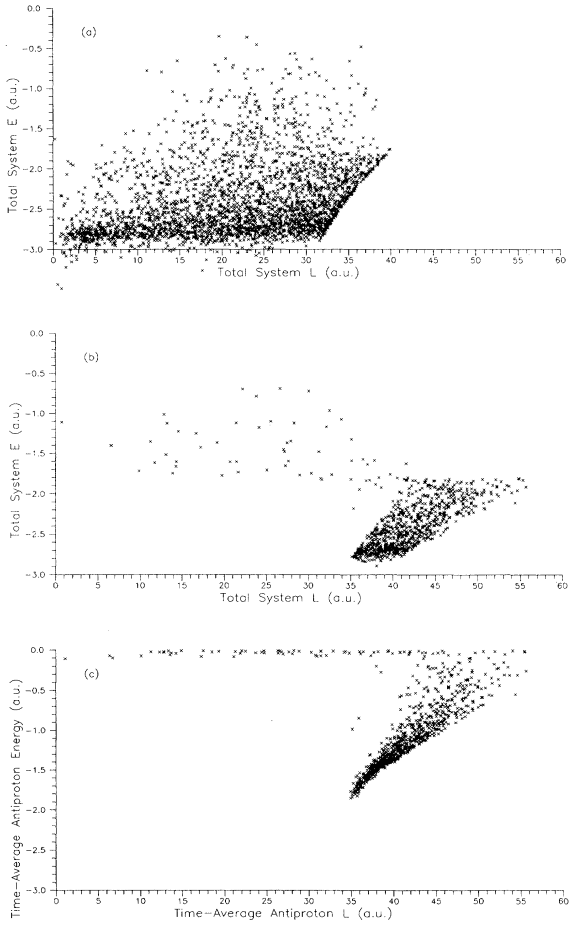

FIG. 4. (a) Final energy and angular momentum for 3 084 $\alpha\bar{p}$ states. (b) Final total system energy and angular momentum for 916 $\alpha e\bar{p}$ states. (c) Time-averaged $\bar{p}$ energy and angular momentum for 916 $\alpha e\bar{p}$ states.

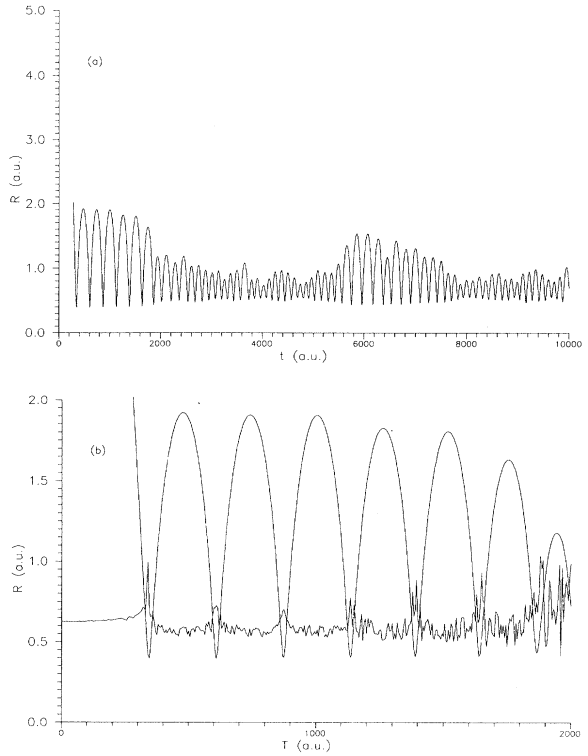

FIG. 5. (a) Radial coordinate of the $\bar{p}$ as a function of time for a particular run, $T_0 = 0.5, b_0 = 0.977$. (b) Radial coordinate of the electron as a function of time, in comparison to a portion of the antiproton trajectory shown in (a). Because of the rapid oscillation of the electron, the figure does not show all of the calculated points.

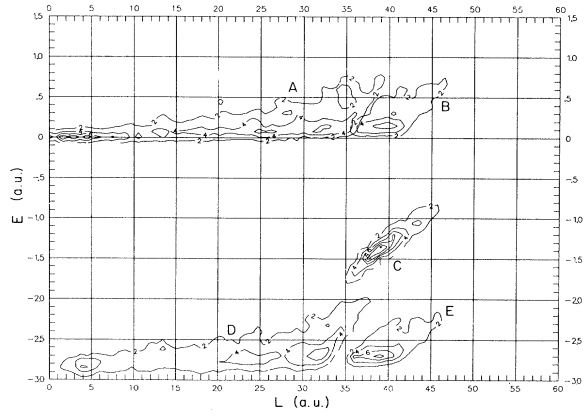

FIG. 6. Density contours, in percent per unit E per unit L. The various regions (islands) describe A: The state of the incident antiprotons for the final collision which ends in capture via double ionization; B: The state of the incident antiprotons for the final collision which ends in capture via single ionization; C: Final (time-averaged) $\bar{p}$, E, and L in the $\alpha e \bar{p}$ configuration; D: Final system states for the $\alpha \bar{p}$ configuration, and E: Final system states for the $\alpha e \bar{p}$ configuration.

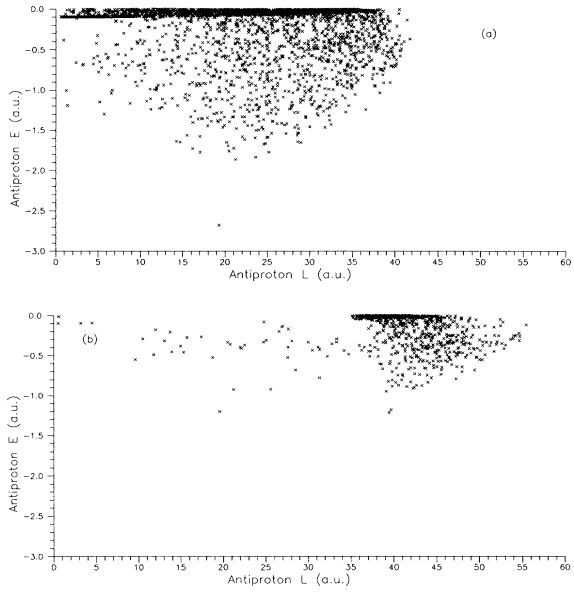

FIG. 7. (a) Energy and angular momentum at initial $\bar{p}$ capture for collisions leading to $\alpha \bar{p}$ products. (b) Energy and angular momentum at initial $\bar{p}$ capture for collisions leading to $\alpha e \bar{p}$ products.

the incident antiprotons with higher angular momentum of Fig. 3(b) clearly separating into the higher angular-momentum states associated with the more stable $\alpha e \bar{p}$ of Fig. 4(b), relative to the lower angular-momentum antiprotons in those systems that will quickly ionize to the $\alpha \bar{p}$ states of Fig. 4(a).

V. CAPTURE ANALYSIS

The quantum antiproton levels for the simple $\alpha \bar{p}$ are given above by Eq. (2). Since $n_0 \approx 38$ has generally been considered the lower limit of the Auger cascade, i.e., the level below which $\bar{p}$ orbits are progressively less disturbed by any electrons which may still be attached, this has been assumed to be the boundary between Auger and radiative decay, where exotic projectiles are expected to accumulate following the Auger cascade before further decay by radiative processes; much below this level decay proceeds primarily by radiative capture irrespective of the state of ionization.

In our calculations, antiprotons captured into $\alpha \bar{p}$ are distributed in this region; Fig. 4(a) shows the antiprotons stacked up against the classical $L = n$ centrifugal boundary in the region of $n \approx 30$–40, with lower L states more heavily populated in the region $n < 35$. It is not surprising that low energy antiprotons are captured into states of $n < n_0$ via double ionization, since the antiproton must exchange enough energy with the atomic electrons to boost both of them into (positive energy) escape from the He nucleus.

It is also generally assumed that the final populations

of these states are distributed according to the statistical factor $2\ell + 1$. Figure 8(a) shows the distribution of the $\alpha\bar{p}$ states vs L/n, where the classical circular angular momentum is given by

$$L_c = n = \sqrt{2M^*/|E|} \ . \tag{11}$$

In this figure, the total L-state distribution, averaged over the different n states, is approximately linear in L.

The separate higher energy and angular-momentum band of $\alpha e\bar{p}$ system states shown in Fig. 4(b) can be compared with the $\alpha e\bar{p}$ system level diagrams proposed by Yamazaki *et al.* [2], shown in Fig. 1; as discussed above, some of the higher-L system states resulting from additional angular momentum contributed by the remaining electron in the singly ionized systems are indeed populated in our calculations.

The distinct, narrow band of high-L excited $\bar{p}$ states present in the singly ionized system [Fig. 4(c)] stack up against a modified centrifugal barrier, at a lower value of L than in the doubly ionized system due to the screening effect of the remaining electron. The degree to which the antiprotons stack up against this barrier is illustrated by the population distribution of Fig. 8(b). Here, the population distribution is plotted against $L/n_{\rm eff}$, where $n_{\rm eff}$, labeling the energy levels of the screened system,

$$E_n = -\frac{Z_{\rm eff}^2 M^*}{2n^2}, \tag{12}$$

is given by

$$n_{\rm eff} = \sqrt{Z_{\rm eff}^2 M^*/E}, \tag{13}$$

with $Z_{\rm eff}$, defined in terms of the central radial force felt by the antiproton

$$F_r = -Z_{\rm eff}/r^2. \tag{14}$$

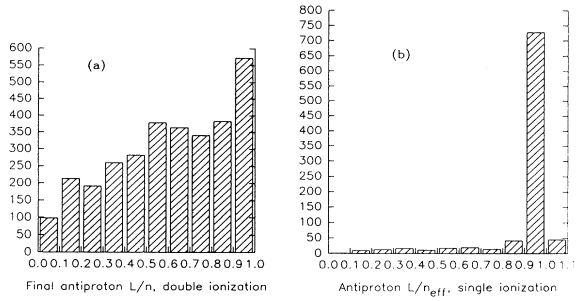

FIG. 8. (a) Distribution in the ratio of angular momentum states L to the classical maximum angular-momentum state $L_{\rm max} = n$ for final $\alpha\bar{p}$ states. Averaging over the different n states shows an approximately linear distribution in the L states populated. (b) Distribution in the ratio of $\bar{p}$ angular-momentum states L to the classical maximum angular-momentum state $L_{\rm max} = n_{\rm eff}$ for final $\alpha e\bar{p}$ states. Averaging over the different n states here shows the concentration in high-L states of the $\bar{p}$'s trapped into $\alpha e\bar{p}$ systems.

VI. METASTABILITY

As discussed above, it is a small percentage of antiprotons in stable, high-L "circular" states, from which the antiproton cannot decay to the point at which it overlaps the nucleus and annihilation occurs, that has been proposed as the source of the observed metastability in long-lived exotic $\alpha e\bar{p}$ atom [1]. In our calculations, a relatively large number of the $\alpha e\bar{p}$ atoms are in these higher-L states; it is, in fact, the higher initial angular momentum of the incident antiprotons which results in their capture via single ionization, as can be seen by comparing the initial antiproton angular momenta, at the start of the collisions resulting in antiproton capture, of Figs. 3(a) (double ionization) and 3(b) (single ionization) with the final system angular-momentum distributions shown in Figs. 4(a) and 4(b).

The question of what constitutes a stable, singly ionized $\alpha e\bar{p}$ system is of course related to how long the system is followed. In our initial calculations, systems were followed for a maximum time of 25 000 a.u., primarily due to limits in computational resources. Indeed, some small fraction of the systems classified as singly ionized have very small binding energy, as can be seen in Fig. 4(c). In most of these cases where the $\bar{p}$ is very loosely bound, the $\bar{p}$ will eventually escape from its exotic system, to be captured by the next He atom it encounters.

To further investigate $\alpha e\bar{p}$ stability in our model, 500 systms were followed to a maximum time of 10^5 a.u. As shown in Fig. 9, the percentage of singly ionized systems surviving on these time scales is well described by a double exponential of the form

$$\begin{aligned} P_{\alpha e\bar{p}}(t) &= P_0 + P_1 e^{-t/\tau_1} + P_2 e^{-t/\tau_2} \\ &= \left[22.3 + 82.6e^{-t/2051} + 7.67e^{-t/57{,}650}\right] \% \ . \end{aligned} \tag{15}$$

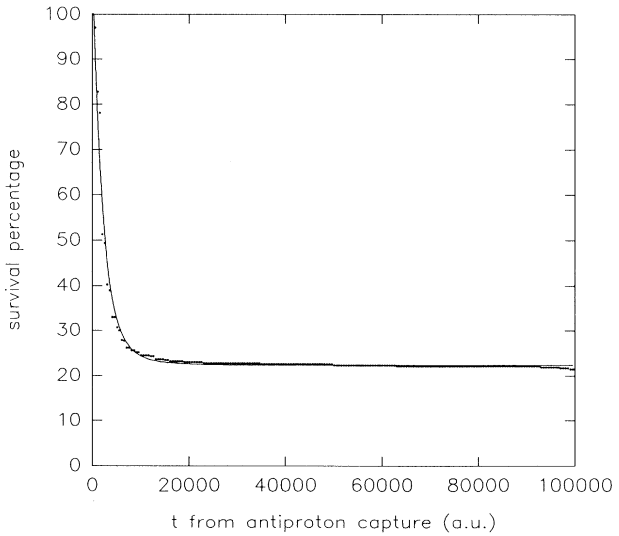

FIG. 9. Survival as a function time of $\alpha e\bar{p}$ systems after initial $\bar{p}$ capture.

This fit gives a survival of 22% up to time 10^5 a.u. compared with the observed metastable population of 3.6% for survival beyond about 1 μs $\approx 4 \times 10^{10}$ a.u. Some decay in the singly ionized population is observed at the end of this time scale, suggesting the existence of additional, longer time scale decay constants for this population.

VII. CONCLUSIONS AND FUTURE

Semiclassical Monte Carlo calculations of the collisions of antiprotons with He offer new details of the slowing and capture processes, including the dependence of the final products on the incoming energy and angular momentum and the state distributions of the singly and doubly ionized exotic $\alpha e\bar{p}$ and $\alpha\bar{p}$ at the end of the Auger cascade. These details shed light on the recently reported metastable states of $\alpha e\bar{p}$.

Further questions to be investigated with this method include the effects of impurities in the target medium on the slowing and capture process, and more detailed study of the Auger process from which the high-L metastable states arise. The population decay of these systems near the end of our time scale invites further study of the dynamics of this decay, and of their relation to the much longer time scales of the metastability discussed by Yamazaki *et al.* [2], who quote mean lifetimes of about 3 μs $\approx 1.25 \times 10^{11}$ a.u., which is beyond the range of our current computational tools.

We can suggest some mechanisms which might reduce survival to 1 μs (which we note is 4×10^5 times our longest runs). One is Stark mixing into s states due to the other helium atoms in the liquid, leading to annihilation on the He nucleus. This is inhibited by the one electron, but may still be significant. Another is annihilation from the higher-L states which we find to survive. We have the population of these states. These could be used by those who have calculated the Born-Oppenheimer states to calculate the annihilation rate from their $\bar{p}$ wave functions at the He nucleus.

ACKNOWLEDGMENTS

The authors are grateful to Professor Toshimitsu Yamazaki for discussions of his work on this problem. This work was supported in part by the DOE; one of us (M.A.A.) was supported in part by the National Science Foundation under Grant No. PHY-9223618.

[1] M. Iwasaki *et al.*, Phys. Rev. Lett. **67**, 1246 (1991).
[2] T. Yamazaki *et al.*, Phys. Rev. Lett. **63**, 1590 (1989).
[3] G. T. Condo, Phys. Lett. **9**, 65 (1964).
[4] J. E. Russell, Phys. Rev. Lett. **23**, 63 (1969); Phys. Rev. **188**, 187 (1969); Phys. Rev. A **1**, 721 (1970); **1**, 735 (1970); **1**, 742 (1970); J. Math. Phys. **12**, 1906 (1971); Phys. Rev. A **6**, 2488 (1972).
[5] C. L. Kirschbaum and L. Wilets, Phys. Rev. A **21**, 834 (1980).
[6] E. Fermi and E. Teller, Phys. Rev. **72**, 399 (1947).
[7] P. K. Haff and T. A. Tombrello, Ann. Phys. (N.Y.) **86**, 178 (1974).
[8] M. Leon, in *Exotic Atoms '79*, edited by K. Crowe, J. Duclos, G. Fiorentini, and G. Torelli (Plenum, New York, 1980), p. 141.
[9] *Electromagnetic Cascade and Chemistry of Exotic Atoms*, edited by L. M. Simons, D. Horvath, and G. Torelli (Plenum, New York, 1990).
[10] M. Karplus, R. N. Porter, and R. D. Shama, J. Chem. Phys. **43**, 3259 (1965).
[11] R. Abrined and I. C. Percival, Proc. Phys. Soc. **88**, 861 (1966); **88**, 873 (1966).
[12] R. E. Olson and A. Salop, Phys. Rev. A **16**, 531 (1977).
[13] J. S. Cohen, Phys. Rev. A **26**, 3008 (1982).
[14] J. S. Cohen, Phys. Rev. A **27**, 167 (1983).
[15] M. Leon and J. H. Miller, Nucl. Phys. A **282**, 461 (1977).
[16] P. Vogel, A. Winther, and V. Akylas, Phys. Lett. **70B**, 39 (1977).
[17] H. Daniel, Phys. Rev. Lett. **35**, 1649 (1975).
[18] P. Vogel, P. K. Haff, V. Akylas, and A. Winther, Nucl. Phys. A **254**, 445 (1975)
[19] M. Leon and R. Seki, Phys. Rev. Lett. **32**, 132 (1974).
[20] M. Leon and R. Seki, Nucl. Rev. A **282**, 445 (1977).
[21] H. Daniel, Z. Phys. **A291**, 29 (1979).
[22] H. Daniel, Ann. Phys. (N.Y.) **129**, 303 (1980).
[23] H. Daniel, Z. Phys. **A302**, 195 (1981).
[24] D. Zajfman and D. Maor, Phys. Rev. Lett. **56**, 320 (1986).
[25] L. Wilets, in *Abstracts of the Eleventh International Conference on the Physics of Electronic and Atomic Collisions, Kyoto, 1979*, edited by K Takayanagi and N. Oda (Society for Atomic Collisions Research, Kyoto, 1979), p. 1008.
[26] P. M. Morse and H. Feshbach, *Methods of Mathematical Physics* (McGraw-Hill, New York, 1953), p. 646, problem 5.3.
[27] I. Shimamura, Phys. Rev. A **46**, 3776 (1992).
[28] T. Yamazaki and K. Ohtsuki, Phys. Rev. A **45**, 7782 (1992).
[29] D. J. E. Callaway, L. Wilets, and Y. Yariv, Nucl. Phys. A **327**, 250 (1979).